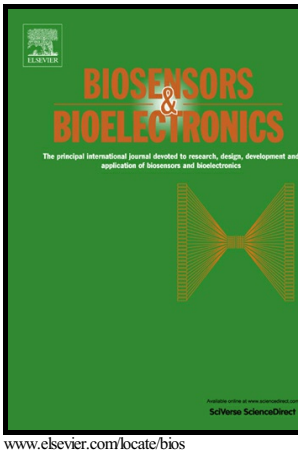

Mixed hemi/ad-micelles coated magnetic nanoparticles for the entrapment of hemoglobin at the surface of a screen-printed carbon electrode and its direct electrochemistry and electrocatalysis

Mohaddeseh Amiri-Aref, Jahan Bakhsh Raoof, Filip Kiekens, Karolien De Wael

www.elsevier.com/locate/bios

PII: S0956-5663(15)30249-9
DOI: http://dx.doi.org/10.1016/j.bios.2015.07.001
Reference: BIOS7818

To appear in: *Biosensors and Bioelectronic*

Received date: 10 May 2015
Revised date: 30 June 2015
Accepted date: 1 July 2015

Cite this article as: Mohaddeseh Amiri-Aref, Jahan Bakhsh Raoof, Filip Kieken and Karolien De Wael, Mixed hemi/ad-micelles coated magnetic nanoparticles for the entrapment of hemoglobin at the surface of a screen-printed carbo electrode and its direct electrochemistry and electrocatalysis, *Biosensors an Bioelectronic,* http://dx.doi.org/10.1016/j.bios.2015.07.001

Mixed hemi/ad-micelles coated magnetic nanoparticles for the entrapment of hemoglobin at the surface of a screen-printed carbon electrode and its direct electrochemistry and electrocatalysis

Mohaddeseh Amiri-Aref [a, b], Jahan Bakhsh Raoof [a], Filip Kiekens[c], Karolien De Wael[b,*]

[a] *Electroanalytical Chemistry Laboratory, Department of Analytical Chemistry, Faculty of Chemistry, University of Mazandaran, Babolsar, Iran*

[b] *AXES, Department of Chemistry, University of Antwerp, Groenenborgerlaan 171, 2020 Antwerp, Belgium*

[c] *Department Pharmaceutics, Campus Drie Eiken, University of Antwerp, 2020 Antwerp, Belgium*

[*]Corresponding author. Tel.: +98 112 5342392; Fax: +98 112 5342350

E-mail address: j.raoof@umz.ac.ir (J.B. Raoof) and karolien.dewael@uantwerpen.be (K. De Wael)

Abstract

An efficient procedure for the physical entrapment of proteins within a biocompatible matrix and their immobilization on electrode surfaces is of utmost importance in the fabrication of biosensors. In this work, the magnetic entrapment of hemoglobin (Hb) at the surface of a screen-printed carbon electrode (SPCE), through mixed hemi/ad-micelles (MHAM) array of positively charged surfactant supported iron oxide magnetic nanoparticles (Mag-NPs), is reported. The Hb/MHAM@Mag-NPs biocomposite is captured at SPCE by a super magnet (Hb/MHAM@Mag-NPs/SPCE). To gain insight in the configuration of the mixed hemi/ad-

micelles of CTAB at Mag-NPs, zeta-potential measurements were performed. The entrapment of Hb at MHAM@Mag-NPs was confirmed by cyclic voltammetry (CV), electrochemical impedance spectroscopy (EIS) and Fourier transform infrared spectroscopy (FT-IR). Direct electron transfer of the Hb intercalated into the composite film showed a pair of well-defined quasi-reversible redox peak at formal potential of -0.255 V vs. Ag/AgCl corresponding to heme Fe(III)/Fe(II) redox couple. It shows that the MHAM@Mag-NPs composite could increase the adsorption ability for Hb, thus provides a facile direct electron transfer between the Hb and the substrate. The proposed biosensor showed excellent electrocatalytic activity to the H_2O_2 reduction in the wide concentration range from 5.0 to 300.0 µM obtained by amperometric measurement. The Michaelis–Menten constant (K_m) value of Hb at the modified electrode is 55.4 µM, showing its high affinity. Magnetic entrapment offers a promising design for fast, convenient and effective immobilization of protein within a few minutes for determination of the target molecule in low sample volume at disposable cost-effective SPCE.

Keywords: Mixed hemi/ad-micelles; Magnetic entrapment; Hemoglobin; Biosensor; Direct electrochemistry; Zeta potential

1. Introduction

Direct electron transfer (DET) of proteins has been a research focus for many years because of its ability to provide a good model for mechanistic studies of electron transfer in biological systems, and its significant role in the field of developing mediator-free bioelectrochemical devices such as third generation biosensors (Gorton et al., 1999; Rusling, 1998), biofuel cells (Ikeda and Kano, 2003; Ramanavicius et al., 2005), heterogeneous catalysts (Vincent et al., 2007) and biomedical devices (Katz and Privman, 2010). Hemoglobin (Hb) is probably the protein whose DET is the most extensively studied. However, redox proteins show

a slow rate of electron transfer on a conventional electrode due to the deep bury of the electroactive prosthetic group, the adsorptive denaturation and the unfavorable orientations when directly adsorbed on the electrode surface (Heller, 1990). Therefore, optimization of the electron transfer between the heme center in the large three-dimensional structure of Hb and the electrode surface is challenging as well as finding ideal electrode materials and suitable protein immobilization methods. For this purpose, entrapment or encapsulation of a protein within a biocompatible material using simple procedures so without the need of complicated covalently attachment or time consuming intermediate step, is certainly desirable.

Biocompatible materials such as natural biomolecules (Paolucci-Jeanjean et al., 2005), biopolymers (Peniche et al., 2003), hydrogels (De Wael et al., 2012), surfactants (Cai and Chen, 2004; Li et al., 2002; Wang et al., 2009) and nanomaterials (Baghayeri et al., 2013; Kafi and Crossley, 2013) would present a favorable microenvironment to keep the activity of the entrapped proteins, and consequently to fabricate eligible biosensors. Considerable attention has been paid in magnetic nanoparticle (Mag-NPs) based electrochemical biosensors in the recent years (Geng et al., 2011; Wang et al., 2013). As an ideal bimolecular immobilizing carrier, Mag-NPs enable quick and efficient isolation or extraction of a target molecule or substance by an external magnetic field (Palecek and Fojta, 2007). Additionally, Mag-NPs can provide a low detection limit due to their large surface area to immobilize biomolecules.

Surfactants can be used as a physical promoter for modifying the nanoparticles. On the other side, the biocompatible characteristics of surfactants would provide a favorable microenvironment to retain the activities of the immobilized proteins (Cai and Chen, 2004). For instance, electrocatalysis of hemoglobin at C_{70}/didodecyldimethylammonium bromide (C_{70}/DDAB) films casted on glassy carbon electrode in an aqueous solution was reported by Li

et al. (Li et al., 2002) and Wang et al. (Wang et al., 2009) studied direct electrochemistry and electrocatalysis of heme proteins with single walled carbon nanotubes-cetyltrimethylammonium bromide (SWCNT/CTAB) nanocomposite film modified glassy carbon electrodes. However, surfactants can make three different coating shells around the Mag-NPs core including hemi-micelle, ad-micelle and mixed hemi-micelle/ad-micelle, which are formed by the adsorption of ionic surfactants on oppositely charged surface of the metal oxides (Merino et al., 2003). In the hemi-micelle state, the adsorbed surfactant molecules spread themselves on the oxides surface to form a monolayer coverage, probably through columbic attraction between the charged Mag-NPs surface and the oppositely charged surfactant head group. With increasing the adsorbed surfactants onto the mineral oxide surface, the hydrophobic interactions between tails of surfactant hydrocarbon chains resulted in the formation of bilayer of surfactant called ad-micelles. Mixed hemi/ad-micelles (MHAM) are an intermediate state between the two previously described terms which is providing a two-fold mechanism for adsorption of amphiphilic analytes (Merino et al., 2003). Major advantage of MHAM respect to the two other states is ability of MHAM in establishing of both electrostatic and hydrophobic interactions with target analytes.

To the best of our knowledge, mixed hemi/ad-micelles supported magnetic nanoparticles (MHAM@Mag-NPs) have not yet been reported, as a protein immobilizing carrier and for direct electron transfer of Hb. For this purpose positively charged surfactant, cetyltrimethylammonium bromide (CTAB), was used for preparing a MHAM coating shell and its formation was controlled by using zeta potential (ZP) measurements. The immobilized Hb at MHAM@Mag-NPs (Hb/MHAM@Mag-NPs) is magnetically entrapped onto disposable screen-printed carbon electrodes (SPCE) via an extremely fast and simple procedure. This magnetic immobilization strategy is employed for the first time as a simple, efficient and disposable cost-effective method

for the preparation of a hemoglobin based biosensor. Finally, integrating the unique properties of MHAM@Mag-NPs with Hb magnetic entrapment allowed an accurate and sensitive determination of hydrogen peroxide in a low sample volume at Hb/MHAM@Mag-NPs/SPCE. The suggested magnetic entrapment offers a promising design for the fast, convenient and effective immobilization of proteins within a few minutes for determination of the target molecule in low sample volume at disposable cost-effective SPCE.

2. Experimental

2.1. Chemical and reagents

The chemical and reagents are described in detail in supplementary information.

2.2. Instrumentation

Electrochemical experiments including cyclic voltammetry (CV), amperometry and electrochemical impedance spectroscopy (EIS) techniques were carried out into a Faraday's cage with an Autolab potentiostat/galvanostat (PGSTAT 302N, ECOCHEMIE, The Netherlands). The experimental conditions for measurements were controlled with Nova software. The morphological characterizations have been examined by means of scanning electron microscopy, SEM (FEI Quanta 250 FEG ESEM, The Netherlands), atomic force microscopy, AFM (Easyscan2 Flex AFM, Switzerland) and transmission electron microscopy, TEM (Zeiss EM10C, Germany). The disposable screen-printed electrodes containing a carbon working electrode (4 mm diameter), a carbon counter electrode and a silver reference electrode were provided from Metrohm, Switzerland . Experiments were performed by introducing a 50 µl drop of PBS onto the SPCE. The SPCE were located in a sealed cubic homemade cell (dimensions: 2×2×1.5 cm3)

and nitrogen atmosphere was assured over the drop during the experiments (Scheme S1). Nitrogen purging was applied to remove oxygen from the measurements medium. To avoid drying of the drop, pure N2 flow (99.99%) was passed through the water container prior to entering the cell. Current-time measurements were performed to quantitatively analyse H2O2 by successive addition of different concentration of H2O2 standard solution under stirring. An Nd-Fe-B strong magnet (magnetic field strength 1.3 Tesla, dimensions 5×5×5 mm3) was used as super magnet. The zeta potential measurements were performed using a Zetasizer apparatus (Malvern 3000, Malvern Instruments Ltd., UK). This instrument determines the electrophoretic mobility of the particles automatically and converts it to the zeta potential. Also, dynamic light scattering (DLS) measurements were performed by the Zetasizer. The pH value of the electrolyte was determined by a digital pH-meter (CyberScan pH 510). An infrared spectrum was obtained using a Fourier transform infrared spectrometer (FT-IR, Bruker Tensor 27 spectrometer, Germany) to identify the functional groups and chemical bonding of the coated materials.

Electrochemical experiments including cyclic voltammetry (CV), amperometry and electrochemical impedance spectroscopy (EIS) techniques were carried out into a Faraday's cage with an Autolab potentiostat/galvanostat (PGSTAT 302N, ECOCHEMIE, The Netherlands). The experimental conditions for measurements were controlled with Nova software. The morphological characterizations have been examined by means of scanning electron microscopy, SEM (FEI Quanta 250 FEG ESEM, The Netherlands) and atomic force microscopy, AFM (Easyscan2 Flex AFM, Switzerland). The disposable screen-printed electrodes with a carbon working electrode (4 mm diameter), a carbon counter electrode and a silver reference electrode were provided from Metrohm, Switzerland. Experiments were performed by introducing a 50 µl drop of PBS onto the SPCE. The SPCE were located in a sealed cubic homemade cell

(dimensions: 2×2×1.5 cm^3) and nitrogen atmosphere was assured over the drop during the experiments. To avoid drying of the drop, pure N_2 flow (99.99%) was passed through the water container prior to entering the cell. Current-time measurements were performed to quantitatively analyse H_2O_2 by successive addition of different concentration of H_2O_2 standard solution under stirring. An Nd-Fe-B strong magnet (magnetic field strength 1.3 Tesla, dimensions 5×5×5 mm^3) was used as super magnet. The zeta potential measurements were performed using a Zetasizer apparatus (Malvern 3000, Malvern Instruments Ltd., UK). This instrument determines the electrophoretic mobility of the particles automatically and converts it to the zeta potential. The pH value of the electrolyte was determined by a digital pH-meter (CyberScan pH 510). An infrared spectrum was obtained using a Fourier transform infrared spectrometer (FT-IR, Bruker Tensor 27 spectrometer, Germany) to identify the functional groups and chemical bonding of the coated materials.

2.3. Synthesis of Mag-NPs

Mag-NPs were synthesized by a published co-precipitation method based on formation of iron oxides from aqueous Fe^{2+}/Fe^{3+} salt solutions in the presence of a base (Zhao et al., 2011); the details of synthesis steps was described in supplementary information.

2.4. Preparation of MHAM@Mag-NPs composite and fabrication of the biosensor

The aqueous suspension of Mag-NPs was prepared by vigorous stirring in pH 9.0 PBS (5 mg/ml). With the isoelectric point at 6.5 (Kosmulski, 2001), iron oxide Mag-NPs have negative surface charges at pH 9.0. Therefore, cationic surfactant CTAB can self-assemble on the surface of negative charged Mag-NPs. To achieve MHAM coating layer on Mag-NPs, the ratio of CTAB

to Mag-NPs concentration is very important and evaluated by zeta potential measurements (section 3.2). A suspension with the optimum concentration ratio of CTAB to Mag-NPs (ratio of 1.5) was prepared at pH 9.0. Then, using a shaker, they were mixed for 5 min to form the suspension of MHAM-coated Mag-NPs. For construction of the biosensing device, 10 μL of the prepared MHAM@Mag-NPs suspension (5 mg/mL) and 10 μL of Hb solution (10 mg/mL, pH 8.5) were mixed for 15 min under gentle stirring. During the shaking, the Hb molecules were adsorbed on the surface of MHAM@Mag-NPs (labeled as Hb/MHAM@Mag-NPs). Since its isoelectric point at about 7.1, Hb is negatively charged at pH 8.5 and could be adsorbed on the positively charged MHAM@Mag-NPs surface, electrostatically Details of the pH and ionic strength effects on the Hb adsorption at MHAM@Mag-NPs were explained in supplementary information. Besides, the hydrophobic part of Hb molecules was involved in hydrophobic chains of the surfactant in the MHAM array. Then, the Hb/MHAM@Mag-NPs were isolated from the suspension by placing an Nd-Fe-B strong magnet (1.3 Tesla) at the bottom side of the vial. Afterward, the supernatant solution was taken out and the captured Hb/MHAM@Mag-NPs (8 μL) were pipetted onto the surface of screen-printed working electrode. The Hb/MHAM@Mag-NPs composite is immobilized at SPCE by applying super magnet underneath the working electrode surface. This set-up allows Hb/MHAM@Mag-NPs to be kept on the working electrode surface by avoiding the use of any complex immobilization step making the whole procedure carried out within a few minutes. The final biosensor is designated as Hb/MHAM@Mag-NPs/SPCE. A schematic diagram of the biosensor apparatus is shown in scheme 1.

Scheme 1

3. Results and discussion

3.1. Characterization of Mag-NPs by AFM, SEM and EDX

According to AFM topography, the mean diameter of the synthesized Mag-NPs is about 88 nm (Fig. 1A). Also, SEM measurements were performed to check the morphology and diameter of Mag-NPs (Fig. 1B). It shows that most of the particles are approximately spherical in shape with the average diameter less than 100 nm which is fitting the AFM data. Additionally, the elemental analysis of sample was examined by EDX spectroscopy which reveals that Fe and O elements are existed in the prepared iron oxide Mag-NPs (Fig. 1C). The existence of Si element in EDX spectrum comes from the substrate of silicon wafer.

Figure 1

3.2. Characterization of MHAM@Mag-NPs and Mag-NPs by TEM and DLS

The results for the TEM and DLS experiments are shown in Fig. S2 and discussed in detail in supplementary information.

3.3. Zeta-potential isotherm studies

The zeta-potential isotherm is a useful tool for understanding the surface-charge characteristics of the particles (Zhao et al, 2011) and finding the region where hemi/ad-micelles of CTAB are formed around the Mag-NPs. Generally, ionic surfactant adsorption isotherms on metal oxides can be divided into three regions (hemi-micelles, mixed hemi/ad-micelles, and ad-micelles) (Atkin et al, 2003). Figure 2 depicts the zeta potential changes of Mag-NPs by adsorptions of different amounts of CTAB. With the isoelectric point at about 6.5, iron oxide Mag-NPs have negative surface charges at pH 9.0 which is favorable for the adsorption of the

cationic surfactants. Therefore, the Mag-NP suspensions were provided at pH 9.0 and the zeta-potential measurements were performed for various ratios of CTAB concentration to the Mag-NP concentration, [CTAB]/[Mag-NP]. As it can be seen in Fig. 2, at first the suspension showed a negative zeta-potential value of -38.6 mV due to the negative charge of the Mag-NPs in a basic media. By changing the ratio of [CTAB]/[Mag-NP] from 0.0 up to 0.9, zeta potentials changed from negative values to zero resulted in formation of CTAB hemi-micelles around the Mag-NPs (monolayer coverage of CTAB on Mag-NPs which allowed only electrostatic interaction). Then, increasing the [CTAB]/[Mag-NP] ratio from 0.9-2.5, the zeta potential converted to positive values and enhanced, due to the positive charge of the CTAB molecules in the second adsorption layer which have been gradually formed. In this region the mixed hemi/ad-micelles are formed having two fold interactions with the amphiphilic molecule, both electrostatic and hydrophobic. However, for the ratio above 2.5, the slope of zeta potential variation was depressed, so making a plateau in isotherm which is assigned to ad-micelles region (all the Mag-NPs were covered by bilayer of CTAB which allowed just hydrophobic attraction). As a consequence, the [CTAB]/[Mag-NP] ratio in the range of 0.9 to 2.5 is the best ratio for immobilization of hemoglobin with the aid of dual interactions. The optimum point in this mixed hemi/ad-micelles region of CTAB for hemoglobin immobilization was determined through cyclic voltammetry experiments (Fig S3) and the [CTAB]/[Mag-NP] ratio of 1.5 was chosen for immobilization of hemoglobin at MHAM@Mag-NP/SPCE. Furthermore, the zeta potential value of 10 mV for the selected ratio indicates the stability of MHAM@Mag-NPs suspension.

Figure 2

3.4. Specifications of Hb/MHAM@Mag-NPs biocomposite by FT-IR

FT-IR spectroscopy was employed to characterize the Hb (a), Hb-MHAM@Mag-NPs (b) and MHAM@Mag-NPs (c) (Fig. S4). The results verified that immobilization of Hb on the surface of MHAM@Mag-NPs did not alter the structure of Hb.

3.5. Electrochemical impedance spectroscopy (EIS) characterization

EIS is a powerful tool to characterize the impedance changes of the electrode surface during the fabrication process and in interaction with the target molecule. The electron transfer resistance (R_{ct}) can be used to describe the interface properties of the electrode which correspond to the electron-transfer kinetics of the redox probe and can be estimated from the diameter of the semicircular domain at higher frequency of the impedance spectra (George and Kee Lee, 2009). Figure 3A represents the Nyquist plot of bare SPCE, MHAM@Mag-NPs/SPCE and Hb/MHAM@Mag-NPs/SPCE in the presence of a negatively charged redox probe, $[Fe(CN)_6]^{3-/4-}$ (1:1). EIS of the bare SPCE shows an approximately straight line (curve a), featuring a diffusion limiting step of the electrochemical processes. At the MHAM@Mag-NPs/SPCE a small semicircle of about 930 Ω with an almost straight tail line is presented (curve b), while immobilization of Hb at the surface of MHAM@Mag-NPs/SPCE was resulted in the increase of the electron transfer resistance, a R_{ct} value of about 1969 Ω (curve c). The increment of R_{ct} can be attributed to two points: 1) Hb in pH 8.5 PBS has remarkable negative charges (above its IEP), which is consistent with the fact that the negatively charged redox probe is electrostatically excreted by the negatively charged state of the Hb molecule, 2) Non-conductive nature of the protein molecules at the electrode surface resulting in the higher electron transfer

resistance for Hb/MHAM@Mag-NPs/SPCE. The results clearly suggest that the Hb was firmly assembled onto the MHAM@Mag-NPs/SPCE. The changed impedance indicates that Hb could be easily adsorbed onto the MHAM@Mag-NPs/SPCE surface by electrostatic interaction of negatively charged Hb and positively charged MHAM@Mag-NPs. It is noteworthy that the presence of Mag-NPs with positively charged mixed hemi/ad-micelles layer of CTAB plays an important role in enhancing the transfer of electrons for MHAM@Mag-NPs/SPCE, and make the electron transfer easier, thus decreasing the resistance of the MHAM@Mag-NPs to $Fe(CN)_6^{3-}$ /$Fe(CN)_6^{4-}$ in comparison with Hb/MHAM@Mag-NPs/SPCE.

3.6. Direct electrochemistry of Hb/MHAM@Mag-NPs/SPCE

Figure 3B depicts cyclic voltammograms of different film modified SPCE in 0.1 M pH 7.0 PBS at a scan rate of 100 mVs^{-1} in deaerated medium. No redox peaks were observed for bare SPCE (curve a) and MHAM@Mag-NPs/SPCE (curve b) in the working potential range, for the latter a large background current could be observed. The background current of MHAM@Mag-NPs/SPCE can be ascribed to the large surface area of the MHAM@Mag-NPs film. When the electrode surface was modified with Hb/MHAM so without magnetic nanoparticles, a pair of weak redox processes appeared (curve c). It is suggested that mixed hemi/ad-micelle array of CTAB can promote the direct electron transfer of Hb to some extent. However, a couple of well-defined and nearly symmetrical redox peaks was clearly observed at Hb/MHAM@Mag-NPs/SPCE with the peak potentials of about −0.29 and −0.22 V corresponding to the Fe (III)/Fe(II) redox couple of the Hb heme center (curve d). The oxidation/reduction peak currents at Hb/MHAM@Mag-NPs/SPCE were larger than those obtained for Hb/MHAM/SPCE, indicating that Mag-NPs in the film could increase the

adsorption capability for Hb and favor the orientation of Hb and thus provide a facile direct electron transfer between the Hb and the electrode. The peak potential difference (ΔE_p) between cathodic peak potential (E_{pc}) and anodic one (E_{pa}) is 70 mV. The formal potential ($E^{o'}$) estimated from the average of E_{pc} and E_{pa} is −0.255 V vs. Ag/AgCl. The ratio of cathodic peak current over the anodic one is close to 1. Based on these data, the direct electrochemistry of Hb in MHAM@Mag-NPs is considered as a quasi-reversible process. In the present work, the MHAM supported Mag-NPs could enhance the adsorption of Hb by introducing dual interactions. One is the electrostatic interactions between the positively charged head groups of mixed hemi/ad-micelles and the negatively charged amino acid residues of Hb (pH 8.5). Another is the hydrophobic interactions between the hydrophobic chains of CTAB in MHAM array and hydrophobic regions of Hb molecule. Therefore, Hb could be intercalated in the mixed hemi/ad-micelles shell around the Mag-NPs and immobilized at the surface of SPCE via an external magnetic field. Finally, the direct electron transfer was achieved between Hb and SPCE surface at the formal potential of -0.255 V.

3.7. Effect of potential scan rate

To further investigate the characteristics of Hb/MHAM@Mag-NPs/SPCE, the effect the potential scan rate was studied. Figure 3C part (a), shows the cyclic voltammograms of the Hb/MHAM@Mag-NPs/SPCE in 0.1 M phosphate buffer (pH 7.0) at different scan rates (from 20 to 200 mV s^{-1}). Figure 3C part (b), illustrates that the anodic and cathodic peak currents (I_p) are increased linearly with the scan rate, as predicted for a surface confined electron transfer process.

The surface concentration of electroactive species (Γ mol cm^{-2}) can be approximately calculated from the slope of peak currents vs. scan rate. For a reversible surface reaction, the peak current has been given by Eq. (1) (Laviron, 1979a):

$$I_p = \frac{n^2 F^2 A \Gamma \upsilon}{4RT} \quad (1)$$

where A is the geometrical surface area of electrode, n is the number of electrons transferred, υ is the potential scan rate and F is the Faraday constant. From the slope of cathodic peak currents vs. scan rate, the calculated surface concentration of Hb was estimated to be 5.00×10^{-10} mol cm^{-2}, which is larger than the theoretical monolayer coverage (1.89×10^{-11} mol cm^{-2}) (Wang et al., 2005). It can be proposed that multilayer of Hb take part in the direct electron transfer process.. The slope obtained by linear regression of log I_p (the logarithm of the peak current) vs. log υ (the logarithm of the potential scan rate) is about 1.08 (Fig.3C part (c)), which is very close to the expected theoretical slope of 1 for thin-layer voltammetry (Bard and Faulkner, 1980). It suggests that all of the electroactive Hb Fe(III) in the film was reduced to Hb Fe(II) on the forward cathodic scan, and subsequently oxidized to Hb Fe(III) on the reverse anodic scan (Moheimanian et al., 2012).

The apparent heterogeneous electron transfer rate constant (k_s) and the transfer coefficient (α) for Hb/MHAM@Mag-NPs/SPCE can be estimated by measuring the variation of the peak potential with the logarithm of the scan rate (Fig.3C part d) based on Laviron's equation (Eq. (2)), derived for a surface-controlled process (Laviron, 1979b):

$$E_{pc} = E^{\circ'} - \left[\frac{2.3RT}{\alpha nF}\right] \log\left\{\left[\frac{\alpha nF}{RT}\right] \times \left[\frac{\upsilon}{K_s}\right]\right\} \quad (2)$$

where

$$Slope = -\frac{2.3RT}{\alpha nF} = S \quad (3)$$

$$Intercepte = E^{\circ'} + S\log\left(\frac{-2.3}{S}\right) - S\log\left(K_s\right) \quad (4)$$

According to Eq (3), the transfer coefficient (α) was calculated as 0.48. The heterogeneous electron transfer rate constant (k_s) was further obtained from Eqs. (3) and (4), and estimated to be 1.69 s^{-1}, which was comparable to those previously reported (Zheng et al., 2009; Shi et al., 2007), indicating that the MHAM@Mag-NPs provided a suitable microenvironment for promoting the electron transfer rate of Hb at the electrode surface.

Figure 3

3.8. Electrocatalytic properties of Hb/MHAM@Mag-NPs/SPCE towards H_2O_2 reduction

The electrocatalytic performance of the Hb/MHAM@Mag-NPs/SPCE towards the reduction of H_2O_2 was evaluated using cyclic voltammetry (CV). Fig. S5 shows cyclic voltammograms of the modified electrode in the absence and presence of H_2O_2. A possible mechanism of reaction of H_2O_2 catalyzed by the Hb/MHAM@Mag-NPs/SPCE is expressed as follows:

$$[HbFe(III) + H^+ + e^- \leftrightarrow [HbFe(II)]$$

$$2\,[HbFe(II) + H_2O_2 + 2H^+ + 2e^- \leftrightarrow 2[HbFe(III)] + 2H_2O$$

The reusability and stability of the proposed biosensor were described in supplementary information. An amperometric measurement is much more accurate and sensitive than cyclic voltammetry for the determination of current, which is usually employed to estimate a lower detection limit. Two linear concentration ranges from 5.0 μM to 60.0 μM and 60.0 μM to 300.0 μM were obtained from the amperometric response of the biosensor (Fig. 4A). The detection

limit from the slope of low concentration range was obtained as 0.6 µM (S/N=3) which is comparable to the other reported Hb modified electrode (Table 1), and the sensitivity was 0.0781 µA μM^{-1}, indicating Hb immobilized at MHAM@Mag-NPs/SPCE exhibited excellent bioelectrocatalytic activity to H_2O_2. The Hb/MHAM@Mag-NPs/SPCE is more sensitive to H_2O_2 at low concentration range, because the calibration plot is steeper in these concentrations than at the higher concentrations. The calibration curve tended to level off when the concentration of H_2O_2 became more than 300.0 µM, exhibiting a characteristic behaviour of the Michaelis–Menten kinetic mechanism (Fig. 4B). The apparent Michaelis–Menten constant ($K_{m),}$ which gives an indication of the enzyme–substrate kinetics, can be calculated from the Lineweaver–Burk equation (Eq. 5) (Li et al., 1996):

$$\frac{1}{I_{ss}} = \frac{1}{I_{\max}} + \frac{K_m}{I_{\max} C} \qquad (5)$$

Here, I_{ss} is the steady-state current after the addition of the substrate, C is the bulk concentration of the substrate and I_{max} is the maximum current measured under saturated substrate solution. K_m can be obtained by the analysis of the slope and the intercept of the plot of the reciprocals of the steady-state current versus H_2O_2 concentration. The Michaelis–Menten constant of the system (K_m) was estimated to be 55.4 µM which is smaller than those of Hb on poly(p-phenylenediamine)@Fe_3O_4/GCE of 88 µM (Baghayeri et al., 2014) and Hb on graphene, flower-like zinc oxide, and gold nanoparticles of 170 µM (Xie et al., 2013). The low K_m value suggests that Hb in MHAM@Mag-NPs composite retains its bioelectrocatalytic activity and exhibits a high affinity to H_2O_2.

Figure 4

Table 1

3.9. Reproducibility, selectivity and real sample analysis

The reproducibility of the proposed disposable biosensor towards H_2O_2 detection was also investigated. The relative standard deviation (RSD) of inter-electrode responses to 60 µM H_2O_2 at three different electrodes was 4.4 % and the RSD of intra-electrode responses to three-times repeated additions of 60 µM H_2O_2 was 5.8%, suggesting acceptable reproducibility of the proposed biosensor. The selectivity of the biosensor was examined in the presence of 10 µM H_2O_2 in 0.1 M PBS (pH=7.0) by addition of the 10-folds concentrations of some interfering compounds such as glucose, ascorbic acid, glycine and tyrosine. These interference compounds at corresponding concentrations (100 µM) did not cause considerable interference and the signal changes were below 6% for H_2O_2 determination (5.8%, 5.2%, 4.1%, and 1.7% for glucose, ascorbic acid, glycine and tyrosine, respectively). The results obviously demonstrate that this sensor has reasonable selectivity. The feasibility of the proposed method in real sample analysis was validated using standard addition method. We applied Hb/MHAM@Mag-NPs/SPCE biosensor in spiked whitening toothpaste (Theramed, Schwarzkopf & Henkel, Düsseldorf-Wien) and human urine samples for a recovery test. As listed in Table S1, the recovery and RSD values indicate that the proposed biosensor is feasible for the analysis of H_2O_2 in real samples.

4. Conclusions

This work present a novel disposable biosensor for hydrogen peroxide based on the immobilization of hemoglobin on the mixed hemi/ad-micelles array of CTAB and magnetic nanoparticles modified screen-printed carbon electrode. By combining the advantage of dual interaction ability of CTAB mixed hemi/ad-micelles and magnetic entrapment ability of the iron oxide magnetic nanoparticle, the Hb/MHAM@Mag-NPs/SPCE biosensor demonstrate a facile

direct electron transfer which confirmed a favorable microenvironment around Hb. This immobilization strategy was performed within a few minutes which is much shorter than other reported immobilization procedures. The Hb/MHAM@Mag-NPs/SPCE exhibited a great affinity towards reduction of hydrogen peroxide with detection limit and Michaelis–Menten constant of 0.6 and 55.4 μM, respectively. The proposed electrochemical biosensor represented the merits of sensitivity, disposable design, cost-effective, low sample volume, fast and simple preparation step that can be useful for third generation biosensor developing.

Acknowledgments

We are thankful for the BOF financial support from the University of Antwerp and Hercules financial support (SEM).

References

Atkin, R., Craig, V.S.J., Wauless, E.J., Biggs, S., 2003. Adv. Colloid Interface Sci., 103, 219–304.

Baghayeri, M., Nazarzadeh Zare, E., Mansour Lakouraj, M., 2014. Biosens. Bioelectron. 55, 259–265.

Baghayeri, M., Nazarzadeh Zare, E., Namadchian, M., 2013. Sens. Actuators, B 188, 227–234.

Bard, A.J., Faulkner, L.R., 1980. Electrochemical Methods: Fundamentals and Applications, Wiley, New York.

Cai, C., Chen, J., 2004. Anal. Biochem. 325, 285– 292.

De Wael, K., Bashir, Q., Van Vlierberghe, S., Dubruel, P., Heering, H.A., Adriaens, A., 2012. Bioelectrochemistry 83, 15–18.

Geng, P., Zhang, X., Teng, Y., Fu, Y., Xu, L., Xu, M., Jin, L., Zhang, W., 2011. Biosens. Bioelectron. 26, 3325–3330.

George, S., Kee Lee, H., 2009. J. Phys. Chem. B 113, 15445–15454.

Gorton, L., Lindgren, A., Larsson, T., Munteanu, F., Ruzgas, T., Gazaryan, I., 1999. Anal. Chim. Acta 400, 91–108.

Heller, A., 1990. Acc. Chem. Res. 23, 128– 134.

Ikeda, T., Kano, K., 2003. Biochim. Biophys. Acta 1647, 121–126.

Kafi, A.K.M., Crossley, M.J., 2013. Biosens. Bioelectron. 42, 273–279.

Katz, E., Privman, V., 2010. Chem. Soc. Rev. 39, 1835–1857.

Kosmulski, M., 2001. Chemical Properties of Material Surfaces, Marcel Dekker, New York.

Laviron, E., 1979a. J. Electroanal. Chem 100, 263–270.

Laviron, E., 1979b. J. Electroanal. Chem. 101, 19–28.

Li, J., Tan, S.N., Ge, H., 1996. Anal. Chim. Acta 335, 137–145.

Li, M., Xu, M., Li, N., Gu, Z., Zhou, X., 2002. J. Phys. Chem. B 106, 4197–4202.

Merino, F., Rubio, S., Perez-Bendito, D., 2003. Anal. Chem. 75, 6799–6806.

Moheimanian, N., Raoof, J. B., Safavi, A., Ojani, R., 2012. Electroanalysis 24, 1386–1393.

Palecek, E., Fojta, M., 2007. Talanta 74, 276–290.

Paolucci-Jeanjean, D., Belleville, M.P., Rios, G.M., 2005. Chem. Eng. Res. Des. 83, 302– 308.

Peniche, C., Argiielles-Monal, W., Peniche, H., Acista, N., 2003. Macromol. Biosci. 3, 511–520.

Ramanavicius, A., Kausaite, A., Ramanaviciene, A., 2005. Biosens. Bioelectron. 20, 1962–1967.

Rusling, J.F., 1998. Acc. Chem. Res. 31, 363–369.

Shan, D., Wang, S.X., Xue, H.G., Cosnier, S., 2007. Electrochem. Commun. 9, 529–534.

Shi, G., Sun, Z., Liu, M., Zhang, L., Liu, Y., Qu, Y., Jin, L., 2007. Anal. Chem.79, 3581–3588.

Vincent, K.A., Li, X., Blanford, C.F., Belsey, N.A., Weiner, J.H., Armstrong, F.A., 2007. Nat. Chem. Biol. 3, 761–762.

Wang, Q., Lu, G., Yang, B., 2004. Sens. Actuators B 99, 50–57.

Wang, S., Xie, F., Liu, G., 2009. Talanta 77, 1343–1350.

Wang, S.F., Chen, T., Zhang, Z.L., Shen, X.C., Lu, Z.X., Pang, D.W., Wong, K.Y., 2005. Langmuir 21, 9260–9266.

Wang, T., Wang, L., Tu, J., Xiong, H., Wang, S., 2013. Bioelectrochemistry 94, 94–99.

Wang, Y.H., Yu, C.M., Pan, Z.Q., Wang, Y.F., Guo, J.W., Gu, H.Y., 2013. Microchim. Acta 180, 659–667.

Wang, Z., Xu, Q., Wang, H.Q., Yin, Z.H., Yu, J.H., Zhao, Y.D. 2009 Anal. Sci. 25, 773–777.

Xie, L., Xu, Y., Cao, X., 2013. Colloids Surf. B 107, 245–250.

Zhang, J., Oyama, M., 2004. Electrochim. Acta 50, 85–90.

Zhao, X., Cai, Y., Wu, F., Pan, Y., Liao, H., Xu, B., 2011. Microchem. J. 98, 207–214.

Zheng, N., Zhou, X., Yang, W.Y., Li, X.J., Yuan, Z.B., 2009. Talanta 79, 780–786.

Figure captions

Fig. 1. (A) AFM image, (B) SEM image and (C) EDX spectra of iron oxide magnetic nanoparticles.

Fig. 2. Zeta-Potential isotherm of Mag-NPs by adsorption of CTAB at pH 9.0.

Fig. 3. (A) Nyquist plots for the faradaic impedance measurements of a 0.01M solution of 1:1 $K_3[Fe(CN)_6]/K_4[Fe(CN)_6]$ performed on (a) bare SPCE, (b) MHAM@Mag-NPs/SPCE and (c) Hb/MHAM@Mag-NPs/SPCE. (B) Cyclic voltammograms of (a) bare SPCE, (b) MHAM@Mag-NPs/SPCE (c) Hb/MHAM/SPCE and (d) Hb/MHAM@Mag-NPs/SPCE in 0.1M PBS pH 7.0 (50 µL) at scan rate of 100 mVs^{-1}. (C) part (a): Cyclic voltammograms of Hb/MHAM@Mag-NPs/SPCE in 0.1M PBS pH 7.0 at different scan rates: (1) 20, (2) 50, (3) 100, (4) 150 and (5) 200 mVs^{-1}; part (b): Plot of peak currents vs. scan rate; part (c): Plot of logarithm of I_{pa} vs. logarithm of υ; and part (d): Plot of peak potentials vs. logarithm of the scan rate (from 20 to 1000 mVs^{-1}).

Fig. 4. (A) Plot of electrocatalytic current vs. H_2O_2 concentration, (B) Plot of the reciprocal of steady-state current (I_{ss}) vs. the reciprocal of H_2O_2 concentration for Hb/MHAM@Mag-NPs/SPCE; based on amperometric response of the biosensor to successive addition of different concentration of H_2O_2 in 0.1 M PBS (pH 7.0) under stirring at constant potential of -0.35 V.

Table 1. Performance of the different H_2O_2 biosensors based on the direct electron transfer of Hb.

Modifier	Electrode	LOD (μM)	Linear range (μM)	Reference
Hb/CdTe-nafion	Glassy carbon	0.84	5–45	Wang et al., 2009
Hb/silica sol–gel	Carbon paste	0.86	1–280	Wang et al., 2004
Hb/nano-Au	Indium tin oxide	4.5	10–7000	Zhang and Oyama, 2004
Hb/Chitosan /nano-$CaCO_3$	Glassy carbon	8.3	37–830	Shan et al., 2007
Hb/Chitosan@Fe_3O_4	Gold	1.1	2.3–9600	Wang et al., 2013
Hb/MHAM@Mag-NPs	Screen-printed carbon	0.6	5-60, 60-300	This work

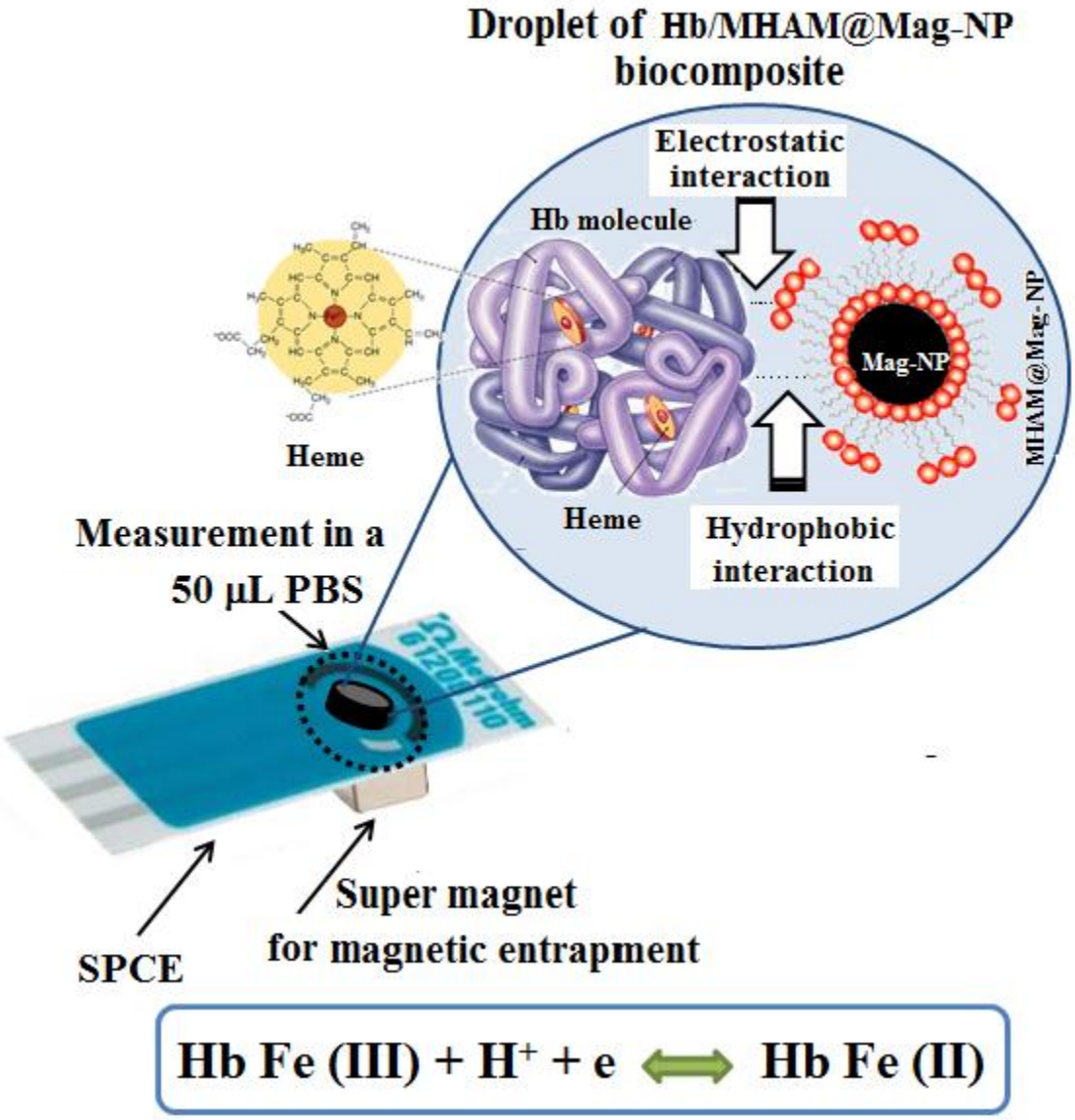
Droplet of Hb/MHAM@Mag-NP biocomposite
Electrostatic interaction
Hb molecule
Mag-NP
MHAM@Mag-NP
Heme
Heme
Hydrophobic interaction
Measurement in a 50 µL PBS
SPCE
Super magnet for magnetic entrapment
Hb Fe (III) + H+ + e ⟺ Hb Fe (II)

Scheme 1

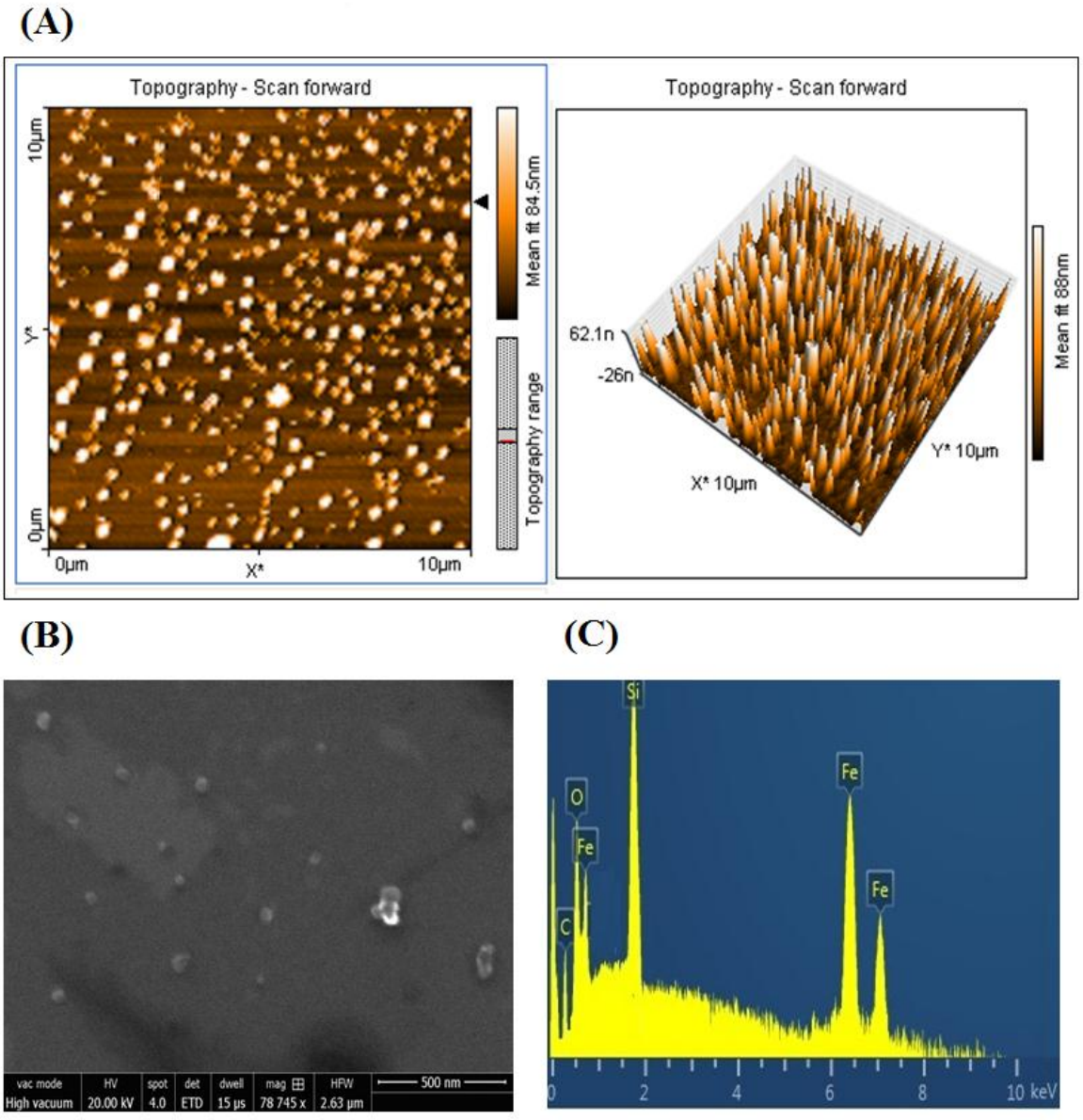
(A)
Topography - Scan forward
10µm
Y*
0µm
0µm
X*
10µm
Mean ft 84.5nm
Topography range
Topography - Scan forward
62.1n
-26n
X* 10µm
Y* 10µm
Mean ft 88nm
(B)
(C)
vac mode
High vacuum
HV
20.00 kV
spot
4.0
det
ETD
dwell
15 µs
mag
78 745 x
HFW
2.63 µm
500 nm
Si
O
Fe
C
Fe
Fe
0
2
4
6
8
10 keV

Fig. 1

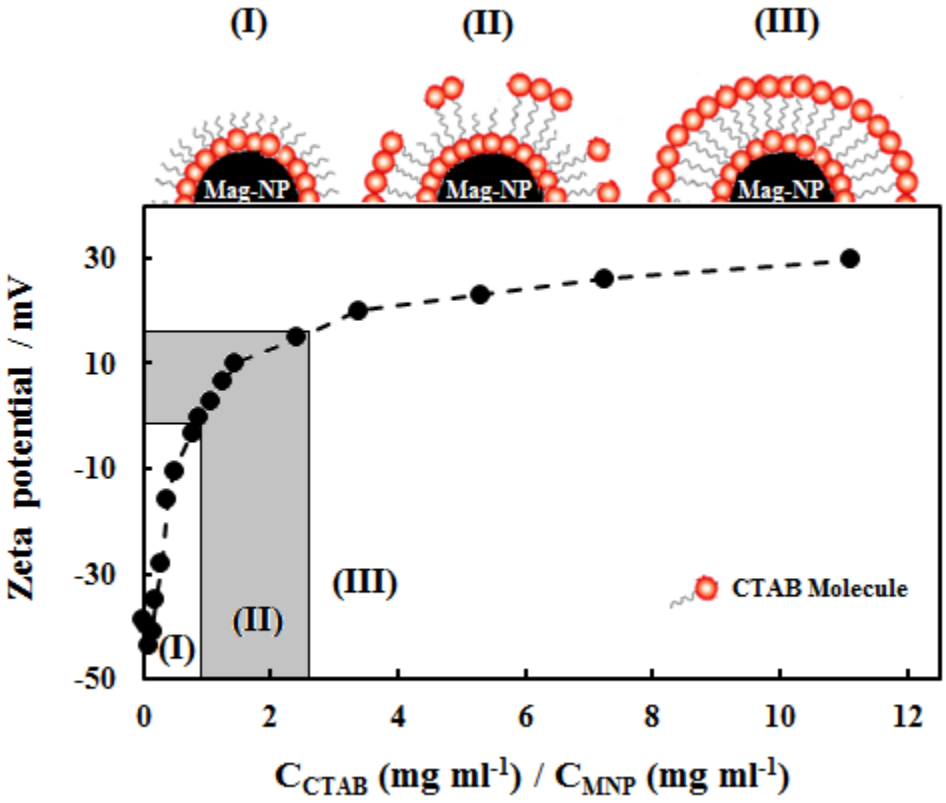
(I)
(II)
(III)
Mag-NP
Mag-NP
Mag-NP
Zeta potential / mV
30
10
-10
-30
-50
0
2
4
6
8
10
12
(I)
(II)
(III)
CTAB Molecule
C_{CTAB} (mg ml^{-1}) / C_{MNP} (mg ml^{-1})

Fig. 2

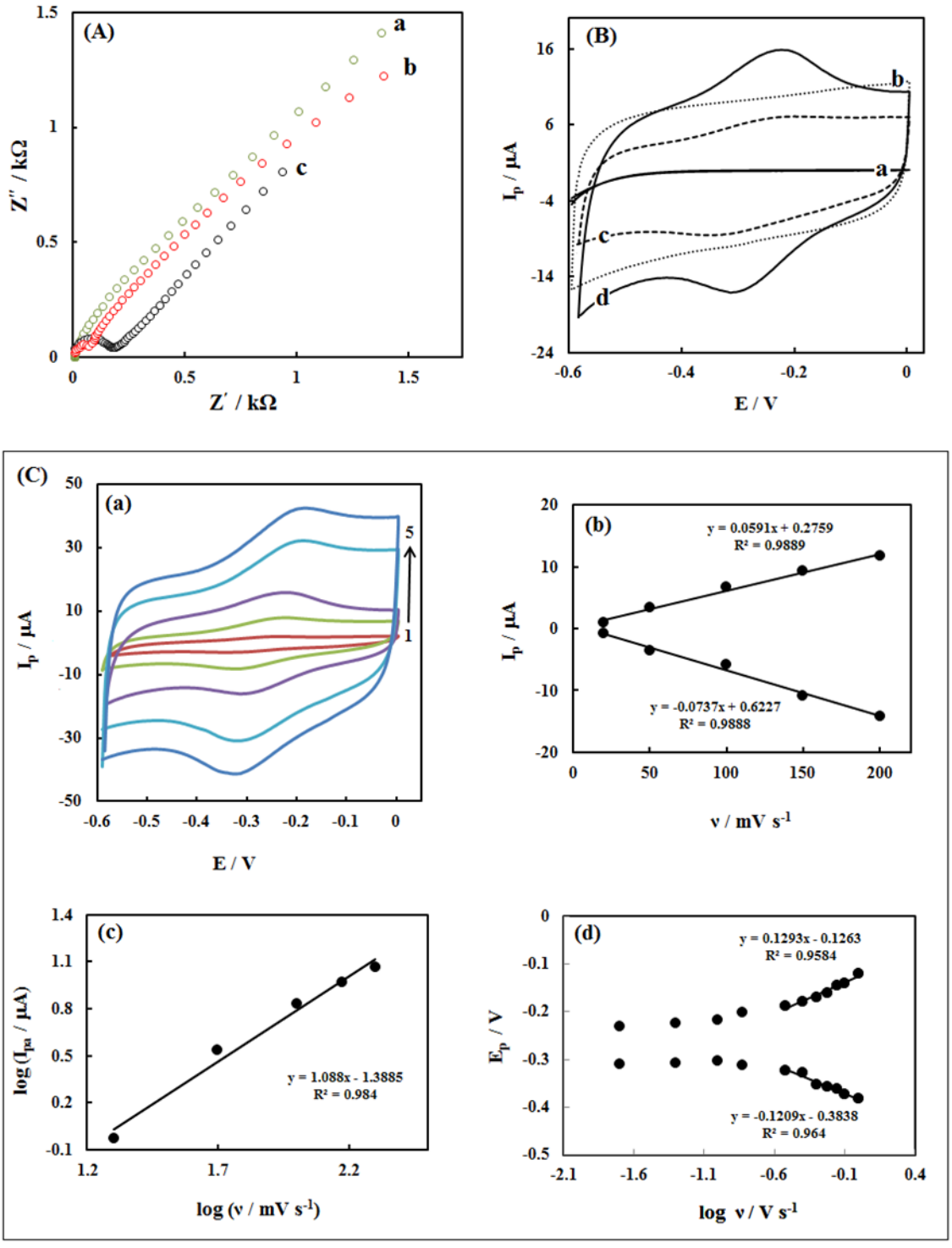
(A)
a
b
c
Z'' / kΩ
Z' / kΩ
(B)
a
b
c
d
I_p / µA
E / V
(C)
(a)
5
1
I_p / µA
E / V
(b)
y = 0.0591x + 0.2759
R² = 0.9889
y = -0.0737x + 0.6227
R² = 0.9888
I_p / µA
ν / mV s^{-1}
(c)
y = 1.088x - 1.3885
R² = 0.984
log (I_{pa} / µA)
log (ν / mV s^{-1})
(d)
y = 0.1293x - 0.1263
R² = 0.9584
y = -0.1209x - 0.3838
R² = 0.964
E_p / V
log ν / V s^{-1}

Fig. 3

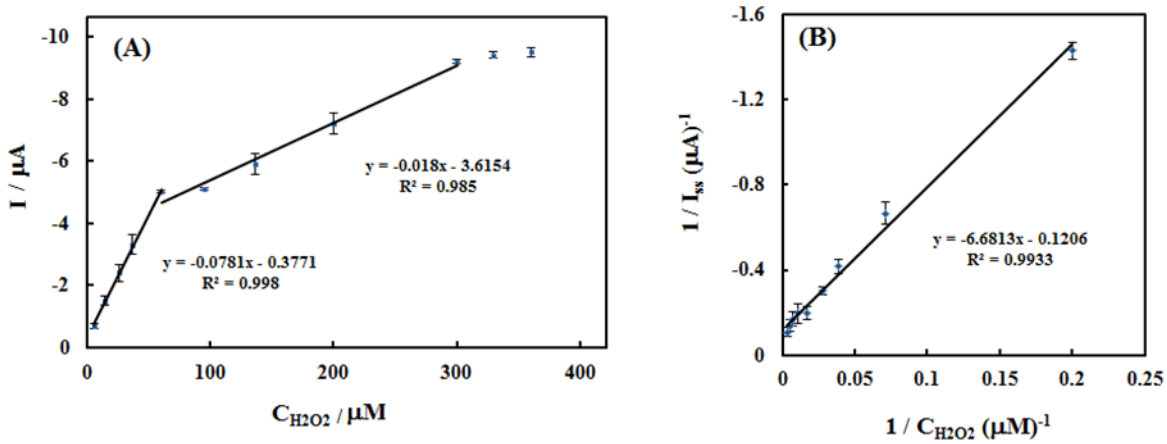

Fig. 4

Research highlights

- A novel disposable H_2O_2 biosensor based on magnetic immobilization of hemoglobin.
- Intercalating hemoglobin in mixed hemi/ad-micelles (MHAM) of CTAB coated Mag-NPs.
- Zeta potential isotherm study was performed to gain the MHAM configuration of CTAB.
- The Hb/MHAM@Mag-NPs biocomposite was captured at SPCE by a super magnet.
- The biosensor exhibited high sensitivity and great affinity towards H_2O_2 reduction.